

**Assessing the Efficacy, Acute Toxicity and Binding Modes of the
Agricultural Nitrification Inhibitors 3,4-Dimethyl-1H-Pyrazole (DMP)
and Dicyandiamide (DCD) With *Nitrosomonas europaea***

Sibel C. Yildirim,^a Robert M. Walker,^b Ute Roessner,^{b,c} Uta Wille*^a

^aSchool of Chemistry, The University of Melbourne, Parkville, Victoria 3010, Australia.

^bSchool of BioSciences, The University of Melbourne, Parkville, Victoria 3010, Australia.

^cResearch School of Biology, The Australian National University, Acton, Australian Capital Territory 2600, Australia.

Corresponding author:

Uta Wille

ph: +61 3 8344 2425; email: uwille@unimelb.edu.au

Abstract

Nitrification inhibitors have been co-formulated with nitrogen fertilizers since the 1970s to modulate the microbiological conversion of nitrogen in agricultural soils. 3,4-Dimethyl-1*H*-pyrazole (DMP) and dicyandiamide (DCD) are currently the most used commercial nitrification inhibitors, but their mode of action is not well understood. This work seeks to fill this void by assessing for the first time in detail their mechanism of inhibition, efficacy, and acute toxicity with pure cell cultures of *Nitrosomonas europaea*. Bacterial assays based on the quantification of the nitrite (NO₂⁻) production showed that both inhibitors reversibly target ammonia monooxygenase (AMO), which catalyzes the first step of the nitrification process. Michaelis-Menten kinetics suggest that both DMP and DCD act as uncompetitive inhibitors. Real-time measurements of the oxygen (O₂) consumption confirmed the non-mechanistic mode of inhibition and showed that DMP reduced the O₂ uptake rate by AMO much more at considerably lower concentrations than DCD, in line with the lower inhibitory efficiency of the latter. Acute toxicity tests revealed that DCD has a 10% higher toxicity than DMP when comparing treatments at the same inhibition efficacy (*i.e.*, DMP at 10 ppm, DCD at 100 ppm), indicating that inhibition of the nitrification process cannot simply be achieved by increasing the inhibitor concentration. The methods presented in this study could assist the development of more reliable nitrification inhibitors in the future.

Keywords

Ammonia monooxygenase; Bacterial assay; Dicyandiamide; 3,4-Dimethyl-1*H*-pyrazole; Inhibition mechanism; Nitrification inhibitor.

Introduction

To meet the food demand of an ever-growing population, the Food and Agriculture Organization of the United Nations (FAO) has predicted that from 2016 – 2022 a 5% increase in nitrogen (N) fertilization from 106 Tg to 112 Tg is required.¹ However, since the 1980s, the N use efficiencies (NUEs) have remained at only around 50% globally.^{2,3} The remaining 50% are lost from the soil through abiotic and biotic pathways, including volatilization of ammonia (NH₃), which is a precursor of particulate matter (PM_{2.5}), and nitrate (NO₃⁻) leaching that causes damaging surface water eutrophication and groundwater pollution.⁴⁻⁶ In addition, microbiological denitrification reduces NO₃⁻ to nitrous oxide (N₂O) and nitric oxide (NO).⁷ N₂O has a 300 times higher global warming potential than CO₂, and mitigation of N losses in agriculture has become an important target for reducing the greenhouse gas (GHG) footprint.⁶

One strategy to improve N management in agricultural soils is to amend N fertilizers with nitrification inhibitors (NIs).^{8,9} Nitrification is caused by ammonia-oxidizing bacteria (AOB) and ammonia-oxidizing archaea (AOA). NIs are small synthetic molecules that are designed to inhibit ammonia monooxygenase (AMO), a multimeric transmembrane enzyme, which is conserved in both AOB and AOA¹⁰⁻¹² and catalyzes the rate-limiting first oxidation step NH₃ → hydroxylamine (NH₂OH).^{13,14} Subsequently, NH₂OH is converted to nitrite (NO₂⁻) by the enzyme hydroxylamine oxidoreductase (HAO),¹⁵ followed by the rapid oxidation to NO₃⁻, the end-product of the nitrification process, which is catalyzed by nitrite oxidase (NXR) present in, for example, *Nitrobacter* spp and *Nitrospira*. In fact, some strains of *Nitrospira* are capable of catalyzing the oxidation from NH₃ to NO₃⁻ (complete ammonia oxidizers, comammox).¹⁶ Furthermore, recent studies revealed that nitrification can also directly lead to formation of NO and N₂O.¹⁷⁻²¹ Thus, by inhibiting AMO, the residence time of NH₃ in soils should be increased, which in turn should reduce N losses through NO₃⁻ leaching and emission of gaseous N compounds produced through both nitrification and denitrification processes. While the crystal structure of AMO remains to be resolved, the evolutionally similar and recently crystallized methane monooxygenase (MMO) has provided some information on the active center in AMO, suggesting that a cupredoxin-like unit could be involved in the oxidation steps.^{10,22-24}

Generally, NIs can be categorized into mechanism-based and non-mechanism-based enzyme inhibitors, such as chelators that coordinate to a metal center in the enzyme's active site without inducing a chemical change.¹³ In contrast, mechanism-based inhibitors are converted in the active site to products that inactivate the enzyme, for example through the formation of covalent bonds. Consequently, recovery of activity of nitrifying bacteria requires *de novo* synthesis of AMO. One prominent example for a mechanism-based NI is the gas acetylene (C₂H₄),^{25,26} but the high flammability and reactivity prohibits its use in agriculture.

Currently commercially available NIs are 3,4-dimethyl-1*H*-pyrazole (DMP), which is commonly applied in agricultural systems as the phosphate salt to reduce its volatility (DMPP or ENTEC®, BASF AG), dicyandiamide (DCD, AlzChem AG) and 2-chloro-6-(trichloromethyl)-pyridine (Nitrapyrin or N-Serve®, Dow Chemical Co.) (Figure 1).

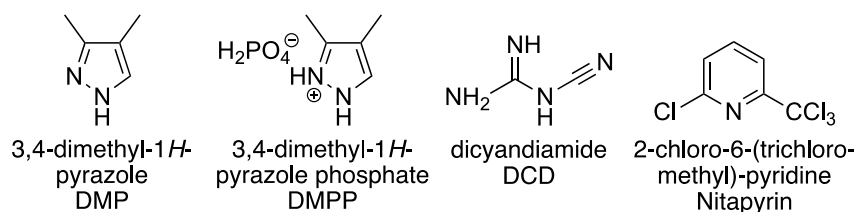


Figure 1. Commercially available nitrification inhibitors (NIs).

Various *in vitro* studies have demonstrated that DMPP reduces nitrification rates; however, field studies revealed that its efficacy strongly depends on the agroecosystem.²⁷⁻³³ DCD, which is widely applied in New Zealand, has been shown to reduce N₂O emissions but is prone to leaching and has been detected in dairy products.³⁴⁻³⁶ Nitrapyrin is highly volatile and is the most intensively studied NI regarding its mode of action.^{37,38} It has been classified as a metal chelator,³⁹ although product analyses indicate that Nitrapyrin could also act as a mechanism-based enzyme inhibitor.³⁷

Despite their widespread use, detailed mechanistic studies are unavailable for DMP (or DMPP, respectively) and DCD. Recently, the crystal structure of six DMP molecules coordinating to a Cu²⁺ center was solved, demonstrating the ligand-binding ability of DMP.⁴⁰ DCD has also been

categorized as a metal-chelator^{12,41-43} and been proposed to act as a competitive inhibitor for AMO.²¹ However, because of the many remaining unknowns of the detailed mode of action of these two NIs, in this work we have performed a comparative study of DMP (as the active component in DMPP) and DCD using assays with pure bacterial cultures of *Nitrosomonas europaea* to determine for the first time important biochemical parameter in the absence of the complex matrix of soil experiments. This study provides crucial insight into the binding mode, efficacy, and acute toxicity of these two commercial NIs, which could help to understand their variable performance in the field and support the development of guidelines to aid the design of next-generation NIs with improved and more consistent performance.

Materials and Methods

1. Chemicals

DMP (3,4-dimethyl-1*H*-pyrazole) was supplied by Incitec Pivot Ltd. Australia. DCD (dicyandiamide) and Griess reagent (modified) was purchased from Sigma Aldrich. Sodium dithionite (Na₂S₂O₄) was obtained from ChemSupply Australia. All aqueous solutions were prepared in Milli-Q water. *N. europaea* (ATCC19718) was purchased from the American Type Culture Collection.

2. Cell Preparation

2.1 Growing *N. europaea* Protocol

AOB were grown for 3 – 5 d in Duran glass bottles containing 600 mL of mineral salts media (MSM, see below) at 100 rpm and 30°C in the dark. The slightly loose cap was sealed with an O₂ permeable membrane to ensure aeration (Breathe-Easy® sealing membrane, Sigma Aldrich). The MSM constituted the main bulk medium and consisted of dipotassium hydrogen phosphate (K₂HPO₄; 2.27 g L⁻¹), potassium dihydrogen phosphate (KH₂PO₄; 0.95 g L⁻¹) and ammonium sulphate ((NH₄)₂SO₄; 0.67 g L⁻¹). The pH was adjusted to 7.0. To 1 L of the bulk medium 2 mL of a filter sterilized (0.2 µm millipore filter) solution of metals was added: disodium ethylenediamine

tetraacetate (Na_2EDTA ; 6.37 g L^{-1}), zinc sulphate heptahydrate ($\text{ZnSO}_4 \times 7 \text{ H}_2\text{O}$; 1.0 g L^{-1}), calcium chloride dihydrate ($\text{CaCl}_2 \times 2 \text{ H}_2\text{O}$; 0.5 g L^{-1}), iron(II) sulphate heptahydrate ($\text{FeSO}_4 \times 7 \text{ H}_2\text{O}$; 2.5 g L^{-1}), sodium molybdate dihydrate ($\text{NaMoO}_4 \times 2 \text{ H}_2\text{O}$; 0.1 g L^{-1}), copper(II) sulphate pentahydrate ($\text{CuSO}_4 \times 5 \text{ H}_2\text{O}$; 0.1 g L^{-1}), cobalt(II) chloride hexahydrate ($\text{CoCl}_2 \times 6 \text{ H}_2\text{O}$; 0.2 g L^{-1}), manganese(II) sulphate monohydrate ($\text{MnSO}_4 \times \text{H}_2\text{O}$; 0.52 g L^{-1}) and magnesium sulphate heptahydrate ($\text{MgSO}_4 \times 7 \text{ H}_2\text{O}$; 60.0 g L^{-1}). To this media solution 1v/v% of aqueous sodium carbonate (Na_2CO_3 ; 50 g L^{-1}) was added aseptically as a carbon source.

2.2 Harvesting Cells Protocol

After 3 - 5 d of incubation, the turbid cultures were harvested at an OD_{600} of approximately 0.1, which represented the mid-exponential growth phase and an NO_2^- production of approximately $800 \mu\text{M}$ (determined by Griess assay), cells were harvested by filtration onto $0.2 \mu\text{m}$ membrane filters (Rowe Scientific, mixed cellulose esters (MCE)). The cells were washed with sodium phosphate buffer (NaPB, pH = 7.5, 0.1 M, 2 x 100 mL) containing MgSO_4 (0.2 mM). The filter paper with the cells was transferred into a sterile 50 mL tube, and the cells were washed off by resuspending in NaPB (15 mL), followed by 5 s of vortexing (Ratek, Australia) and 3 s of sonication (Vevor, Australia). The initial inoculum OD_{600} , which was between 0.9 – 1.2, was adjusted to a final OD_{600} of 0.03 and stored at 4°C until used for the assay. Cells could be stored for up to 24 h without losing activity.

3. Nitrification Assay and Analysis

3.1 Standard Assay Protocol

In a deep 96-well plate (2 mL capacity), $980 \mu\text{L}$ of the bacterial inoculum ($\text{OD}_{600} = 0.03$ in NaPB at pH 7.5) was added to the inhibitor ($10 \mu\text{L}$ of a 30 mmol L^{-1} or 3 mmol L^{-1} stock solution, respectively), the solutions were mixed thoroughly and pre-incubated in the dark for 5 min at 30°C and 100 rpm (Ratek, Australia). $(\text{NH}_4)_2\text{SO}_4$ ($10 \mu\text{L}$, 150 mM, from a sterile solution containing 19.8 g L^{-1} of $(\text{NH}_4)_2\text{SO}_4$ in Milli-Q water) was then added. In experiments in which the NH_2OH -

dependent activity was measured, $(\text{NH}_4)_2\text{SO}_4$ was replaced by equimolar amounts of NH_2OH . The plate was covered with an O_2 permeable membrane to ensure aeration (Breathe-Easy® sealing membrane, Sigma Aldrich) and incubated in the dark for 30, 60 or 90 min at 30°C and 100 rpm. The nitrification process was stopped by adding an excess of DMP ($10 \mu\text{mol L}^{-1}$, 30 mM; the final concentration of DMP in the solution was 0.27 mM, which was considerably higher than the $\text{IC}_{50\text{abs}}$ value of 6.6 μM determined previously).⁴⁴ An aliquot of the reaction solution (50 μL) was transferred to a 96-well spectrophotometric plate (Greiner Cellstar®, polystyrene) to which 50 μL of Griess reagent was added. The color was allowed to develop for 15 min at room temperature, and the absorbance was measured at 540 nm (Clariostar® BMG Labtech, Australia). Each assay was accompanied by control treatments to determine the 0% and 100% NO_2^- signal. The percentage inhibition was calculated according to eqn. (1) from the NO_2^- production of the cells in NaPB (i) without additive ("untreated cells"; 0% signal), (ii) with $[\text{NH}_4^+] = 3 \text{ mM}$ ("uninhibited cells"; 100% signal) and (iii) with $[\text{NH}_4^+] = 3 \text{ mM}$ and $[\text{inhibitor}] = 0.3 \text{ mM}$ (10 mol% of $[\text{NH}_4^+]$; "inhibited cells").

$$\% \text{ Inhibition} = \left[1 - \frac{[\text{NO}_2^-]_{\text{inhibited cells}} - [\text{NO}_2^-]_{\text{untreated cells}}}{[\text{NO}_2^-]_{\text{uninhibited cells}} - [\text{NO}_2^-]_{\text{untreated cells}}} \right] \times 100 \quad (\text{eqn. 1})$$

3.2 O_2 Consumption Measurements

O_2 consumption rates of cell suspensions of *N. europaea* were measured using a Clark-type oxygen electrode (Rank Brothers, Cambridge, UK) mounted in a water-jacketed electrode chamber (3 mL capacity) that was connected to a recirculating cooler (Lauda, Austria). The data were recorded using a Data-trax™ (World Precision Instruments, UK) sensor data collection system. All measurements were taken at 20°C and 1 mL final reaction solution volume (the lower temperature, compared to the other experiments in this study that were performed at 30°C, was required here to increase signal stability). The polarizing voltage was set to 0.6 V. To calibrate the oxygen signal, an excess (approximately 50 mg) of $\text{Na}_2\text{S}_2\text{O}_4$ was added to 1 mL of Milli-Q water to chemically remove dissolved O_2 . Additional O_2 flux was prevented by applying a stopper, and the residual voltage was referred to as "0% O_2 ". The voltage at saturated O_2 concentration ("100%

O₂) was determined by measuring the voltage of the equilibrated aerated reaction system consisting of 1 mL Milli-Q water. Sample measurements were taken as follows: The 1 mL reaction mixture, composed of 980 µL *N. europaea* cell solution in NaPB (OD₆₀₀ = 0.8; corresponding to approximately 468 µg L⁻¹ protein) was equilibrated for 5 min in the chamber until the voltage reading was stable. The reaction was then initiated by the addition of (NH₄)₂SO₄ (10 µL of an aqueous 150 mM stock solution, the final concentration in the reaction solution was 3 mM) and the chamber immediately sealed with a stopper. After 5 min of oxygen consumption (a linear rate coefficient of approximately 186 ± 63 nmol O₂ L⁻¹ s⁻¹ was determined), 10 µL of the inhibitor stock solution of DMP (0.012 mM, 0.12 mM, 0.6 mM, 1.2 mM) or DCD (1.2 mM, 2.0 mM, 5.0 mM, 10.0 mM) were added via a 10 µL Eppendorf pipette through a capillary opening, ensuring the emergence of the pipette tip in the solution. The voltage was recorded over a period of 5 min in intervals of 5 s. The trace describing the O₂ concentration after addition of (NH₄)₂SO₄ against the time (initial 15-300 s) was used as the baseline O₂ consumption for the uninhibited cells, whereas the trace describing the consumption in the presence of the inhibitor (300-590 s time window) was used to determine the rate of O₂ consumption in the presence of inhibitor. All experiments were conducted in triplicate at 20°C under constant stirring. The voltage was converted to [O₂] according to equation 2:⁴⁵

$$[O_2]_t = \frac{\text{voltage (sample)}_t - \text{voltage (0\% O}_2)}{\text{voltage (100\% O}_2) - \text{voltage (0\% O}_2)} \times 280 \mu\text{M} \quad (\text{eqn. 2})$$

3.3 Activity Recovery Assay

Cells were harvested using the 'Harvesting Cells Protocol'. The bacteria solution was adjusted to OD₆₀₀ = 0.8 (~ 468 µg L⁻¹ protein), and 980 µL aliquots were transferred to 1.5 mL centrifuge tubes (Eppendorf®, polypropylene). The inhibitor (10 µL of a stock solution of 150 mM in Milli-Q water) was added, and after equilibrating for 5 min (NH₄)₂SO₄ (10 µL of a stock solution of 150 mM in Milli-Q water) was added using a multichannel pipette to ensure simultaneous addition in each tube. The tubes were incubated in a temperature-regulated rotary incubator (Ratek, Australia) for 30 min at 30°C and 100 rpm in the dark. A 50 µL aliquot was then transferred to a 96-well plate (Greiner Cellstar®, polystyrene) to which 50 µL of Griess reagent was added and the mixture

incubated for 15 min. The absorbance was measured at 540 nm (Clariostar® BMG Labtech, Australia). The remaining cells were subsequently washed (3x) by alternating centrifuging (Boeco, Germany; 10,000 rpm, 10 min) and resuspending the cell pellet in NaPB (1 mL). After the final centrifuging step, the pellet was resuspended in NaPB (990 µL) and re-incubated with (NH₄)₂SO₄ (10 µL of an aqueous 150 mM stock solution, see above), and the NO₂⁻ concentration was measured under the previously described conditions. Each assay was accompanied by control treatments to determine the 0% and 100% NO₂⁻ signal. The %activity was determined according to equation 3, where "untreated cells" (0% signal) is the NO₂⁻ production of the cells without additive, "uninhibited cells" (100% signal) the NO₂⁻ production of cells treated with [NH₄⁺] = 3 mM, and "inhibited" cells" the NO₂⁻ production of cells treated with [NH₄⁺] = 3 mM and [inhibitor] = 1.5 mM. All experiments were performed in triplicate.

$$\% \text{ Activity} = 1 - \frac{[\text{NO}_2^-]_{\text{inhibited cells}} - [\text{NO}_2^-]_{\text{untreated cells}}}{[\text{NO}_2^-]_{\text{uninhibited cells}} - [\text{NO}_2^-]_{\text{untreated cells}}} \quad (\text{eqn. 3})$$

3.4 Michaelis-Menten Kinetics

In a deep 96-well plate (2 mL capacity), 980 µL of the bacterial inoculum (OD₆₀₀ = 0.03, ~ 18 µg L⁻¹ protein in NaPB at pH 7.5) was added to DMP (10 µL from 0.75 mM and 1.5 mM stock solutions, respectively) or DCD (10 µL from 15 mM and 30 mM stock solutions, respectively). The solutions were mixed thoroughly and pre-incubated in the dark for 5 min at 100 rpm and at 30°C (Ratek, Australia). 10 µL of the respective (NH₄)₂SO₄ stock solution (150 mM, 75 mM, 5 mM, 2.5 mM, 1.5 mM, 0.15 mM) was added to each well (final [NH₄⁺] in well: 3.0 mM, 1.5 mM, 0.1 mM, 0.05 mM, 0.03 mM, 0.003 mM). The plate was covered with an O₂ permeable membrane to ensure aeration (Breathe-Easy® sealing membrane, Sigma Aldrich) and incubated in the dark for 60 min at 30°C and 100 rpm. Termination of the nitrification process and determination of the NO₂⁻ production was performed as described in 'Standard Assay Protocol'. Data analysis was performed with the GraphPad Prism software, using nonlinear regression (curve fit) for Michaelis Menten Kinetics.⁴⁶ The results used the best fit values with 95% likelihood.

3.5 Acute Toxicity Test

Cells were harvested according to 'Harvesting Cells Protocol'. The bacteria solution was adjusted to $OD_{600} = 0.8$ ($\sim 468 \mu\text{g L}^{-1}$ protein) and divided into 1 mL aliquots. To each well of a 24-well tissue culture plate (Greiner Cellstar®, polystyrene Tissue Culture treated) was added 980 μL of bacterial solution, 10 μL of a 150 mM aqueous $(\text{NH}_4)_2\text{SO}_4$ solution and 10 μL of either a DMP or a DCD solution with a final concentration in the well of 10 ppm (0.015 mM), 100 ppm (0.15 mM) and 1000 ppm (1.5 mM), respectively. The well plate was sealed with an O_2 permeable membrane to ensure aeration (Breathe-Easy® sealing membrane, Sigma Aldrich) and incubated in the dark for 4 h at 30°C and 100 rpm. Cells were then transferred into a centrifuge tube and sedimented at 10,000 rpm for 10 minutes. The supernatant was separated, and the cells were re-suspended in NaPB (pH = 7.5, 1 mL). A 5 μL aliquot was transferred into a 96-well plate and the bacterial stain (LIVE/DEAD™ BacLight™ Bacterial Viability Kit for microscopy, ThermoFisher Scientific) was added following the manufacturer's instructions. 10 μL of the solution was transferred onto a microscopic slide (Fisher Scientific, Australia, microscope slides 7.6 cm x 2.5 cm (L x W), thickness 1 - 1.2 mm). Seven images were taken per treatment with a fluorescent microscope (Leica DM6000, Germany) using the red channel to detect dead cells (excitation: 575/30 nm (dichromatic) DC: 600; emission: 635/40 nm) and the green channel to detect live cells (excitation: 500/20 nm DC: 515; emission: 535/30 nm). The percentage of live and dead cells was calculated via equations 4 and 5:

$$\% \text{ Live} = \frac{\text{Live cell count}}{\text{total cell count}} \times 100 \quad (\text{eqn. 4})$$

$$\% \text{ Dead} = \frac{\text{Dead cell count}}{\text{total cell count}} \times 100 \quad (\text{eqn. 5})$$

Prior to the microscopic imaging, 50 μL of supernatant was reacted with 50 μL Griess reagent to determine $[\text{NO}_2^-]$ following the 'Standard Assay Protocol'.

4. Statistics

Statistical analysis was performed with the GraphPad Prism software⁴⁶ using student's t-test $P < 0.05$ as the level of statistical significance. All results are reported as mean \pm standard error of the mean. In addition, significances among three treatments were compared by the least significant differences $P < 0.05$ level using one-way ANOVA.

Results and Discussion

We first identified the enzyme targeted by DMP and DCD and their mode of binding using *N. europaea* as model AOB. The analysis was performed by measuring the amount of NO_2^- produced in the absence and presence of the NI, which was determined using a recently developed assay based on the Griess reaction.⁴⁴ We then explored the mode of inhibition by measuring the Michaelis-Menten kinetics and the inhibitory efficacy by establishing the rate of NH_3 oxidation by *N. europaea*, which was obtained from O_2 consumption measurements. Analysis of the acute toxicity of both inhibitors was performed to investigate whether the lower production of NO_2^- in the presence of DMP and DCD could be due to a potential toxicity of the inhibitors for the bacteria.

Identification of the enzyme targeted by DMP and DCD

As outlined in the Introduction, oxidation of NH_3 to NO_3^- occurs in several steps, where AOB are responsible for the first two steps, *i.e.*, $\text{NH}_3 \rightarrow \text{NH}_2\text{OH} \rightarrow \text{NO}_2^-$, which are catalyzed by the enzymes AMO and HAO, respectively. While DMP and DCD are believed to target AMO, to our knowledge, no study is currently available that unequivocally confirms this hypothesis. Thus, to explore, which of these two enzymes is inhibited by DMP and DCD, we performed assays where pure cell cultures of *N. europaea* were treated in sodium phosphate buffer (NaPB) at pH 7.5 and 30°C separately with either NH_4^+ (as substrate for AMO) or NH_2OH (as substrate for HAO) and measured the cumulative NO_2^- production over 90 min in the presence and absence of the NI. Inhibition of the enzyme should result in a lower NO_2^- production, compared to the non-inhibited cell culture. The concentration of the N source (provided as $(\text{NH}_4)_2\text{SO}_4$ or NH_2OH , respectively)

was 3 mM, and the inhibitors were supplied at two different concentrations (*i.e.*, 1 mol% and 10 mol% of applied N). Figure 2 shows the production of NO_2^- over 90 min under the different conditions. Control experiments, which were performed with cells in NaPB without N source and inhibitor, did not reveal a notable production of NO_2^- , confirming that NO_2^- resulted from oxidation of NH_4^+ or NH_2OH , respectively. The detailed data are provided in Tables S1 and S2 in the Supporting Information (SI).

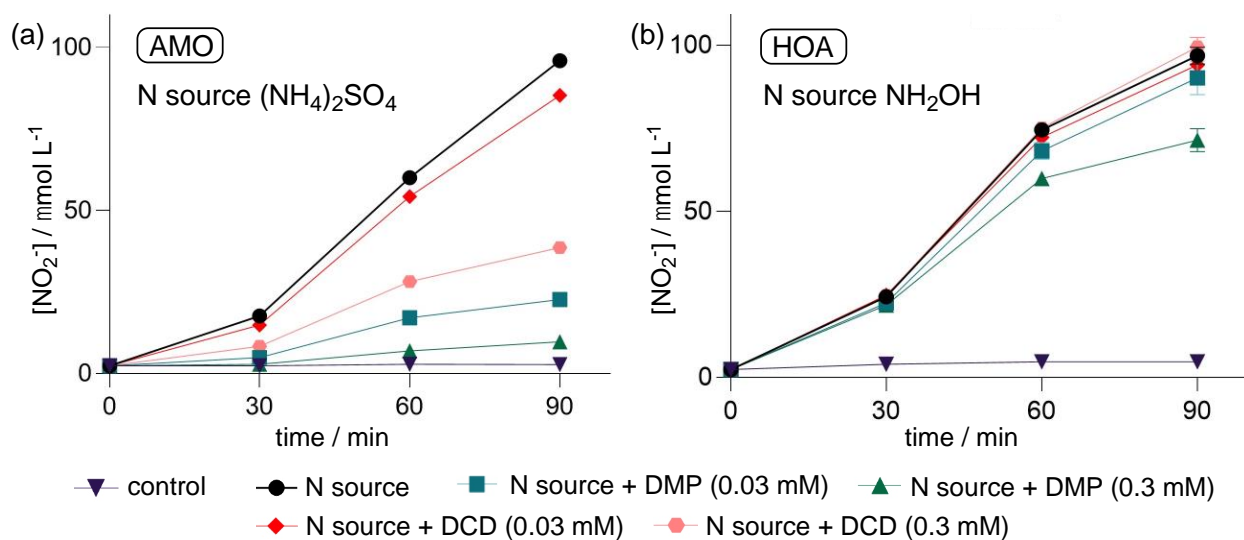


Figure 2. (a) Effect of DMP and DCD at different concentrations on the cumulative NO_2^- production after 30 min, 60 min and 90 min of inoculation with (a) $[\text{NH}_4^+] = 3 \text{ mM}$ and (b) $[\text{NH}_2\text{OH}] = 3 \text{ mM}$ as N source, respectively. The inoculations were performed in NaPB (pH = 7.5) at 30°C and 100 rpm in the dark. Standard errors were calculated from three biological replicates, each performed with three technical replicates.

In the incubations targeting AMO (Figure 2(a)) uninhibited cells generated a total $[\text{NO}_2^-]$ of 17.7 μM after 30 min, corresponding to an NO_2^- production rate of about 0.5 $\mu\text{M min}^{-1}$. Over the next 60 min the activity of AMO increased to an average NO_2^- production rate of 1.3 $\mu\text{M min}^{-1}$. Treatment with both DMP and DCD reduced the NO_2^- production when compared to the uninhibited cells, however, the inhibiting effect was generally more pronounced with DMP than with DCD at the same concentration, in agreement with literature data.^{47,48} Thus, in the first 30

min, cells exposed to 0.03 and 0.3 mM of DMP produced $[\text{NO}_2^-]$ of 4.9 and 2.9 μM , respectively. Compared to the uninhibited cells, the %inhibition (calculated according to equation (1)) was 83% for 0.03 mM DMP and 93% for the ten-fold higher concentration. Over the following 60 mins the %inhibition with $[\text{DMP}] = 0.03 \text{ mM}$ decreased to 74%, whereas with $[\text{DMP}] = 0.3 \text{ mM}$ the %inhibition remained unchanged at 94%. In contrast, the inhibitory performance of DCD depended much stronger on its concentration. After 90 mins, the %inhibition with $[\text{DCD}] = 0.03 \text{ mM}$ was only 11%, whereas with $[\text{DCD}] = 0.3 \text{ mM}$ the %inhibition was 61%.

Providing NH_2OH to the cell culture enabled to study the HAO catalysed transformation, *i.e.*, $\text{NH}_2\text{OH} \rightarrow \text{NO}_2^-$, under exclusion of AMO. Figure 2(b) shows that uninhibited cells produced around the same amount of NO_2^- after 90 min as those treated with NH_4^+ . Treatment of the cells with DMP at the lower concentration and with DCD at both concentrations had practically no impact on the NO_2^- production. Only when the cells were exposed to 0.3 mM of DMP, a noticeable reduction of $[\text{NO}_2^-]$ occurred, which amounted to a %inhibition of about 27% after 90 min. However, we do not believe that the lower NO_2^- production at higher $[\text{DMP}]$ indicates HOA inhibition but is likely an indirect effect of the strong AMO inhibition. As AMO accepts two electrons from HOA that are produced during the oxidation of NH_2OH , AMO inhibition could disrupt the electron transfer chain between these two enzymes, thereby reducing HOA activity. With regards to the 'fate' of both NIs in AMO, it is unlikely that they undergo conversion in the enzyme to produce a more active form, as no increase in %inhibition over time was observed. This finding suggests that both DMP and DCD are chelators (*i.e.*, non-mechanism based enzyme inhibitors) that could coordinate to the Cu^{2+} centers in AMO through their N atoms *via* a vacant electron pair, as has been found in crystal structures of the DMP-Cu^{2+} and the DCD-Cu^{2+} complexes.^{43,49} However, it cannot be excluded that the inhibitory effect of DMP and DCD could, at least in part, be due to a potential toxicity for AMO. We will explore this factor below.

Determining the inhibition mechanism

To gain mechanistic insight how DMP and DCD are inhibiting AMO, we studied the Michaelis-Menten kinetics by measuring the production of NO_2^- at different $[\text{NH}_4^+]$ and constant $[\text{NI}]$. The Michaelis constant, K_m , is the substrate concentration, $[\text{S}]$, at which the reaction rate, v , is 50%

of the maximal rate V_{\max} and can be regarded as an inverse measure of the enzyme-substrate affinity (see equation 6).

$$v = \frac{V_{\max} [S]}{K_m + [S]} \quad (\text{eqn. 6})$$

Thus, non-competitive inhibition is characterized by a decrease of V_{\max} that is independent of $[S]$, as substrate and inhibitor are not competing for the same site in the enzyme (K_m unchanged). In contrast to this, uncompetitive inhibition shows both a decreased K_m and V_{\max} , whereas competitive inhibition shows an increased K_m and an unchanged V_{\max} .⁵⁰

[DMP] and [DCD] were chosen close to their $IC_{50\text{abs}}$ values (DMP: 6.6 μM and DCD: 0.1 mM)⁴⁴ to achieve partial inhibition (50 – 80%) of the NO_2^- production. Figure 3 shows that formation of NO_2^- followed Michaelis-Menten-type saturation kinetics for both inhibitors, clearly revealing that not only less NO_2^- was produced in the presence of the inhibitor but that increasing $[\text{NH}_4^+]$ beyond 1.5 mmol L^{-1} did not have any impact on $[\text{NO}_2^-]$.

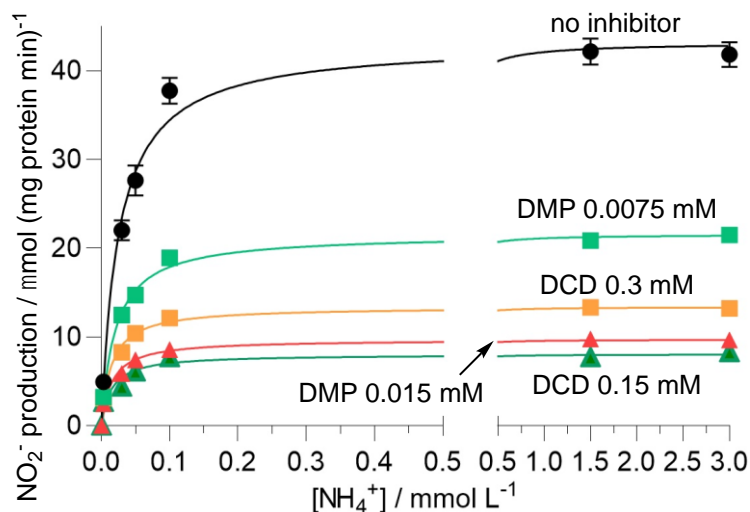


Figure 3. Effect of DMP and DCD on the NO_2^- production in dependence of $[\text{NH}_4^+]$ after 60 min. The inoculations were performed with $[\text{NH}_4^+] = 0.003 \text{ mM}, 0.03 \text{ mM}, 0.05 \text{ mM}, 0.1 \text{ mM}, 1.5 \text{ mM}$ and 3.0 mM in NaPB (pH = 7.5) at 30°C and 100 rpm in the dark. Note the different axis scale to include the data at higher $[\text{NH}_4^+]$. Standard errors were calculated from three biological replicates.

Apparent half-saturation constants for ($K_{m(\text{app})}$) and maximum velocities ($V_{\text{max}(\text{app})}$) in the presence/absence of DMP and DCD were calculated using the hyperbolic regression analysis (see section 3.4 in Materials and Methods). Note that the prefix 'app' (apparent) was used as these studies were performed with bacterial cells and not with the pure enzyme. The data are shown in Table 1.

Table 1. Michaelis Menten kinetics parameter of the $[\text{NH}_4^+]$ dependent production of NO_2^- by *N. europaea* in the absence and presence of DMP or DCD, respectively, at different concentrations.^a

Inhibitor	Concentration / mM	$V_{\text{max}(\text{app})} / \mu\text{mol (mg protein min)}^{-1}$	$K_{m(\text{app})} / \mu\text{M}$
none	--	43.2 ± 1.2	25.4 ± 1.8
DMP	0.0075	21.6 ± 0.2	20.5 ± 0.2
	0.015	9.7 ± 0.3	15.1 ± 1.9
DCD	0.15	13.4 ± 0.3	14.4 ± 0.7
	0.3	8.0 ± 0.3	14.4 ± 4.7

^a[NI] were selected to achieve partial inhibition of the NO_2^- production and amended according to their efficacy (see text). Standard errors were calculated from three biological replicates, each performed with three technical replicates.

Compared to uninhibited cells, DMP and DCD reduce $V_{\text{max}(\text{app})}$ by about 50 - 85%. Furthermore, $K_{m(\text{app})}$ for both inhibitors is significantly lower ($P < 0.05$) than for the uninhibited cells. These findings suggest that both DMP and DCD inhibit pure bacterial cultures of *N. europaea* through uncompetitive inhibition.

Although the crystal structure of AMO, particularly its active site, is unknown, simulations of bacterial AMO revealed that the enzyme contains multiple Cu^{2+} containing subunits.^{12,51} DMP and DCD could principally bind to any of these sites, depending on accessibility. However, as

uncompetitive inhibitors bind to the enzyme-substrate complex to show an inhibitory effect, it is highly likely that the inhibitor binding site is near the substrate binding site.

Exploring the reversibility of the inhibition

Next, we explored whether the inhibition of AMO by DMP or DCD is reversible or irreversible. For these experiments, *N. europaea* cells were incubated for 30 min with 3 mM of NH_4^+ and a high concentration of DMP or DCD, respectively ($[\text{NI}] = 1.5 \text{ mM}$), to ensure considerable inhibition, and the NO_2^- production was measured ("inhibited cells"). The cells were then washed several times with NaPB with the intention to remove both unbound and enzyme-bound inhibitor. After the final washing cycle, NH_4^+ was added to the cells, and the NO_2^- production was measured again after 30 min of incubation. The %activity was determined according to equation 3 (details are provided in section 3.3 in Materials and Methods). The data are shown in Table 2.

Table 2. Determination of the activity of inhibited AMO, using pure cell cultures of *N. europaea*, and after removal of the NI through repeated washing with NaPB.^a

Inhibitor	%Activity	
	inhibited cells	after washing
DMP	4.2 ± 2.6	66.6 ± 3.3
DCD	32.6 ± 7.3	54.6 ± 13.0

^aThe inoculations were performed with $[\text{NH}_4^+] = 3.0 \text{ mM}$ and $[\text{DMP}]$ or $[\text{DCD}] = 1.5 \text{ mM}$ in NaPB (pH = 7.5) at 30°C and 100 rpm in the dark. Standard errors were calculated from three biological replicates, each performed with three technical replicates.

In the first step of the experiment, cells exposed to DMP showed an activity of about 4% (nearly quantitative inhibition due to the high $[\text{DMP}]$ used), whereas in the case of DCD the nitrification activity of the cells was reduced to about one-third, re-confirming that DMP is a more efficient inhibitor than DCD. After washing the cells and re-incubation with NH_4^+ , the activity increased to

67% for the cells previously treated with DMP and to 55% for the DCD treated cells. The considerable recovery of enzyme activity after washing the cells, particularly in the case of DMP, suggests reversible inhibition, whereas irreversible inhibitors form covalent bonds with the enzyme, requiring *de novo* synthesis of AMO to regain activity. For example, nitrifying cells exposed to the irreversible inhibitors acetylene and 1-octyne recovered their activity only after four hours.⁵² Binding studies performed with Nitapyrin showed that the release of the inhibitor required washing of the cells with buffer containing Cu^{2+} to 'force' de-complexation of the NI from AMO.³⁸ In the case of DMP and DCD, however, washing the cells with buffer solution alone was sufficient to remove the inhibitors from the enzyme, suggesting that their coordination to the relevant Cu center(s) in AMO is not very strong, which could provide a rationale for the variable performance of these NIs in the field. The finding that no full recovery of activity was observed is not surprising, given the high inhibitor concentration used in this experiment, which could lead to the partial loss of cells (see below).

Determination of the rate of NH_3 oxidation by AMO

The rate of the NH_3 oxidation by AMO and whether NIs directly target this process can be determined through O_2 respiration measurements. As NH_3 oxidation requires equimolar O_2 , the O_2 consumption (or O_2 uptake by the enzyme) is directly proportional to the NH_3 oxidation rate.⁵³ We measured the O_2 consumption by cell suspensions of *N. europaea* at 20°C using a Clark-type oxygen electrode by first monitoring the decrease of $[\text{O}_2]$ in the presence of NH_4^+ (3 mM) for 5 min. The inhibitor was then added at different concentrations, the system was allowed to equilibrate for 15 s, and the O_2 decay was subsequently monitored for a further 5 min. In all measurements, NH_4^+ and O_2 were both present in excess so that the rate was only determined by the enzyme concentration (the total protein concentration was $\sim 468 \mu\text{g L}^{-1}$, determined via a BCA assay kit). Under these conditions, the O_2 consumption should follow zero-order kinetics, and the rate coefficient, k , can be determined from the slope of the plot of $[\text{O}_2]$ over time. In the presence of inhibitor, NH_3 oxidation should slow down, resulting in a slower rate of O_2 consumption. It should be noted that the inhibitor concentrations were chosen such that the O_2

consumption was not completely stopped. Thus, to compensate for the lower efficacy of DCD, the latter required higher concentrations than DMP.

Figure 4(a) shows the O₂ consumption of cells treated with DMP, and Figure 4(b) that for DCD treated cells.

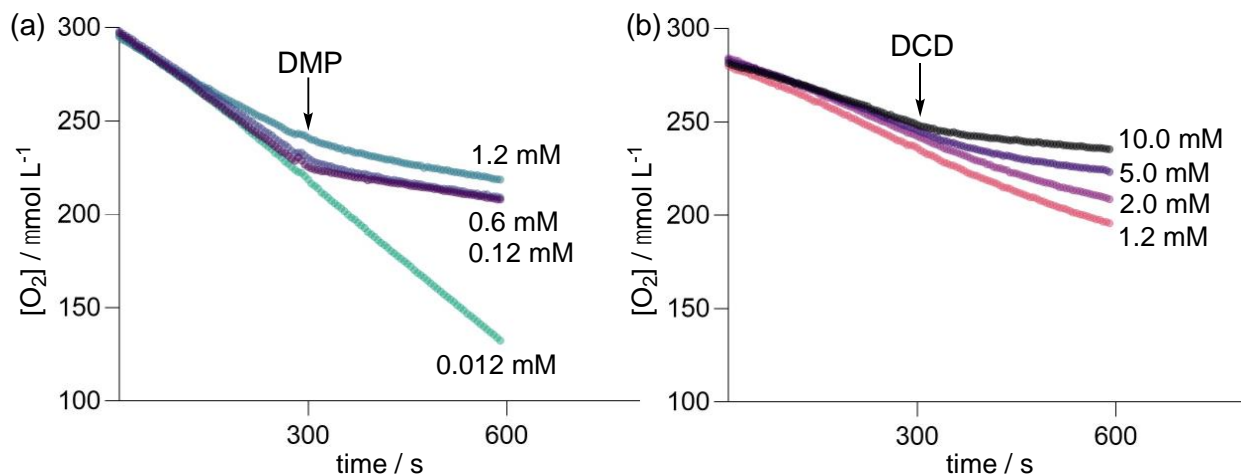


Figure 4. Measurements of the O₂ consumption by *N. europaea* in the absence and presence of (a) DMP and (b) DCD at different concentrations. The first 300 s is the rate in the absence of inhibitor. At the 300 s timepoint the inhibitor was added (indicated with an arrow). The cells were treated with [NH₄⁺] = 3.0 mM at pH = 7.5 at 20°C under constant stirring in the dark. The plot shows the mean of three measurements for each concentration; standard errors are omitted for clarity.

In the initial stage of the experiment in the absence of inhibitor, the measured linear dependence of the O₂ consumption over time confirmed zero-order kinetics, revealing a rate coefficient of $186 \pm 63 \text{ nmol L}^{-1} \text{ s}^{-1}$ (see Table S3 and Figure S1). The rate of O₂ consumption slowed down after addition of the inhibitors, as would be expected for a reduced enzyme activity, but remained zero order (see Figures S2 and S3). Table 3 compiles the rate coefficients for the O₂ consumption in the absence and presence of the NIs. The data for each replicate measurement are compiled in Table S4.

Table 3. Rate coefficient, k , for the O₂ consumption by *N. europaea* in the absence and presence of DMP and DCD, respectively, and the %inhibition at different [NI].^a

Inhibitor	Concentration / mM	k / nmol L ⁻¹ s ⁻¹	%Inhibition
none	--	186 ± 63	--
DMP	0.012	199 ± 117	no inhibition
	0.12	31 ± 13	75 ± 6
	0.6	64 ± 9	65 ± 5
	1.2	56 ± 1	70 ± 1
DCD	1.2	118 ± 20	28 ± 6
	2.0	112 ± 9	40 ± 7
	5.0	68 ± 9	63 ± 5
	10.0	39 ± 9	79 ± 5

^aCells were treated with [NH₄⁺] = 3.0 mM in NaPB (pH = 7.5) at 20°C under constant stirring in the dark. All errors are standard errors calculated from three measurements of biological replicates. %Inhibition determined according to: 100 - [rate (with inhibitor) / rate (without inhibitor) x 100].

The zero-order behavior in the presence of DMP and DCD supports our findings from the previous sections that both NIs are chelating agents that reversibly bind to the enzyme. In contrast, mechanism-based inhibitors, such as acetylene and phenylacetylene, bind irreversibly to the enzyme, which reduces the enzyme's 'active' concentration over time and results in a first-order consumption of O₂ by the enzyme.^{54,55}

Overall, cells treated with DCD consumed more O₂ than cells treated with DMP, although [DCD] was considerably higher than [DMP], clearly confirming that both inhibitors, although with different efficiency, directly impact on the ability of AMO to promote NH₃ oxidation. The %inhibition at the different [NI] could be obtained from the ratio of the rate coefficients in the presence and absence of the inhibitor, which are included in Table 3. Thus, the %inhibition by DMP was relatively constant in the concentration range 0.12 - 1.2 mM, averaging to 70 ± 4%. In contrast, the %inhibition by DCD was considerably more concentration dependent, dropping from 79% for 10 mM to just 28% for 1.2 mM.

Determination of short-term toxic effects of DMP and DCD

A bacterial viability stain can provide insights of toxic effects of chemical compounds for *N. europaea*. While this method has been previously used to explore the toxicity of silver nanoparticles for *N. europaea*,⁵⁶ no such evaluation has been done for NIs.

To assess the acute toxicity of DMP and DCD for *N. europaea*, cells were incubated at 30°C in NaPB (pH = 7.5) with $[\text{NH}_4^+] = 3 \text{ mM}$ for 12 hours with three different concentrations of DMP and DCD (10 ppm, 100 ppm and 1000 ppm). Figure 5 shows two exemplary microscopic images for *N. europaea* bacterial cells without inhibitor and with $[\text{DMP}] = 10 \text{ ppm}$. It should be noted that the incubations in the absence of inhibitor were also performed with $[\text{NH}_4^+] = 3 \text{ mM}$ to avoid cell death caused by starvation. Standard errors were determined from seven microscopic images. The numbers of life/dead cells for each image are provided in Table S5.

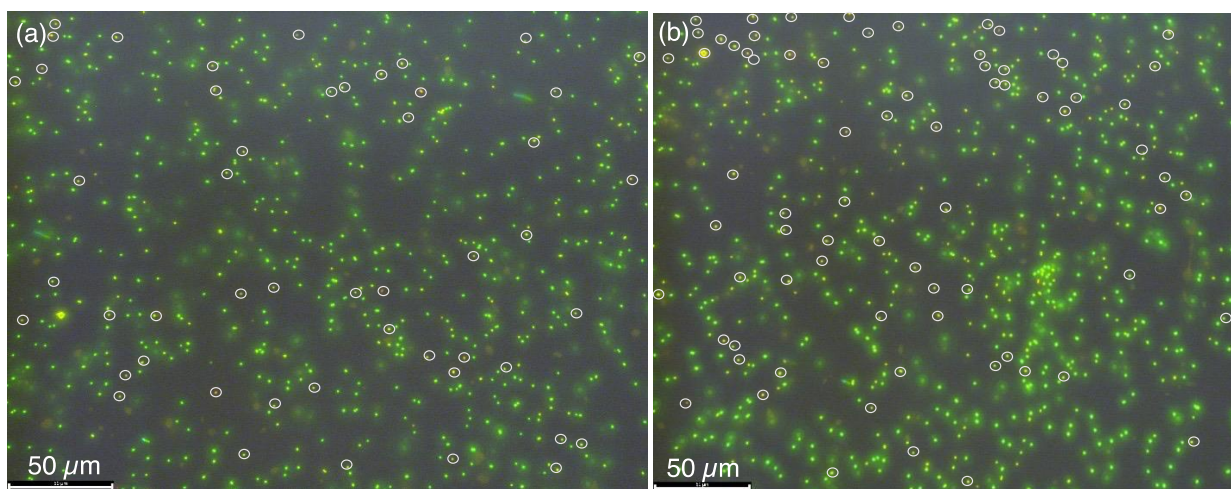


Figure 5. Microscopic images of *N. europaea* in the (a) absence of DMP and (b) presence of 10 ppm DMP. The cells were visualized with the BaCLight™ viability stain. Channels were overlaid to show 'alive' cells (green) and 'dead' cells (red) in a single image. Note that the dead cells (which are in the minority) appear orange in these images, which have been circled for clarity.

Table 4 shows the percentage of live and dead cells (calculated using eqn. 5 and 6) at the different concentrations of the NI.

Table 4. Acute toxicity of DMP and DCD at different concentrations for cells of *N. europaea* determined with a bacterial viability stain and determination of the NO_2^- production.^a

Inhibitor	Concentration / ppm	% Live	% Dead	$[\text{NO}_2^-] / \mu\text{M}$
none	--	96 ± 3	5 ± 3	454
DMP	10	87 ± 9	7 ± 7	338
	100*	70 ± 8	29 ± 5	112
	1000*	67 ± 5	34 ± 5	46
DCD	10	89 ± 4	10 ± 4	430
	100*	77 ± 15	22 ± 15	444
	1000*	74 ± 11	25 ± 11	445

^aThe incubations were performed in NaPB at pH = 7.5 and 30°C with $[\text{NH}_4^+] = 3 \text{ mM}$, $[\text{inhibitor}] = 10 \text{ ppm}$ (0.015 mM), 100 ppm (0.15 mM) and 1000 ppm (1.5 mM) at 100 rpm for 12 h in the dark. Standard errors were determined from seven microscopic images; * indicates significant difference in comparison to uninhibited cells ($P < 0.05$).

At the lowest concentration (10 ppm), cell death caused by both NIs was non-significant compared to the control treatment. However, both inhibitors decreased the %live cells when their concentration was increased to 100 ppm, *i.e.*, 70% for DMP and 77% for DCD, respectively. With $[\text{inhibitor}] = 1000 \text{ ppm}$, 74% of cells treated with DCD remained alive, whereas the toxicity of DMP was higher, with just 65% of the cells still alive. Parallel to the viability stain, the NO_2^- production was also measured, which showed that the higher cell death rate with increasing [DMP] correlated with a reduction of $[\text{NO}_2^-]$. In contrast, in the case of DCD the NO_2^- production remained largely unchanged at all three concentrations (even in comparison with the control treatment), which further confirms the much lower inhibitory activity of this inhibitor.

However, when assessing inhibitor efficiency and toxicity, it needs to be considered that an at least ten times higher application rate of DCD would be required to achieve a nitrification inhibition comparable with DMP (see Figure 1). For example, while with [DMP] = 10 ppm no significant cell death occurs, the cell death is much higher for [DCD] = 100 ppm. Therefore, increasing the application rate of DCD is not a useful approach to increase nitrification inhibition, as it would lead to increased cell death.

In conclusion, using pure cell cultures of *N. europaea* we have shown that DMP and DCD target the first step of nitrification by inhibiting AMO. Although at higher concentrations of DMP the NO_2^- production through NH_2OH oxidation mediated by HOA decreased too, we suggest that this reduction is an indirect effect of the strong AMO inhibition. Both inhibitors can be removed from the enzyme by washing with buffer, indicating that they act as chelating agents, which reversibly bind to the enzyme. These findings were confirmed by measuring the kinetics of the O_2 consumption by *N. europaea* in the presence of DMP and DCD, respectively. DMP reduced the O_2 uptake rate considerably more at much lower concentrations than DCD, in line with the lower inhibitory efficiency of the latter. However, the binding between enzyme and NIs is not very strong, which may, at least to some extent, explain the highly variable performance of both NIs in different soils,²⁷⁻³³ and could provide a potential pathway to develop more efficient and consistent NIs in the future. Furthermore, Michaelis-Menten kinetics revealed that both DMP and DCD act as uncompetitive inhibitors, whereas studies of the acute toxicity suggest that increasing the application rate of the poorer performing DCD to increase inhibition of AMO cannot be recommended as it is associated with increased cell death. On a final note, it has been shown that temperature is also a crucial factor affecting inhibitory efficiency, as more rapid degradation of the nitrification inhibitors could occur in soils at higher temperatures.^{21,57,58} In future work, we will therefore apply the bacterial assay used here to explore in detail the role of temperature on the inhibitory activity through kinetic studies.

Abbreviations Used

AMO – ammonia monooxygenase

ANOVA – Analysis Of Variance

AOA – ammonia oxidizing archaea

AOB – ammonia oxidizing bacteria

ATCC – American Type Culture Collection

BCA – bicinchoninic acid

DCD – dicyandiamide

DMP – 3,4-dimethyl-1*H*-pyrazole

DMPP – 3,4-dimethyl-1*H*-pyrazole phosphate

HAO – hydroxylamine oxidoreductase

FAO – Food and Agriculture Organization of the United Nations

GHG – greenhouse gas

IC_{50abs} – concentration of inhibitor to decrease response to 50%

K_m – Michaelis-Menten constant

MSM – mineral salts media

NaPB – sodium phosphate buffer

NI – nitrification inhibitor

N. europaea – *Nitrosomonas europaea*

NUE – nitrogen use efficiency

OD – optical density

OD₆₀₀ – optical density at 600 nm

PM_{2.5} – particulate (diameter ≤ 2.5 μm)

ppm – parts per million

rpm – rotations per minute

SI – supporting information

UV/vis – ultraviolet visible region

V_{\max} – maximal rate

Supporting Information

Supplementary Table S1 (Cumulative NO_2^- production by *N. europaea* with ammonium (NH_4^+) in the absence and presence of DMP and DCD over three consecutive 30-min intervals); Table S2 (Cumulative NO_2^- production by *N. europaea* with hydroxylamine (NH_2OH) in the absence and presence of DMP and DCD over three consecutive 30-min intervals); Table S3 (Rate coefficients, k , for the time-dependent O_2 consumption by *N. europaea* in the absence of NI); Table S4 (Rate coefficients, k , for the time-dependent O_2 consumption by *N. europaea* in the presence of DMP and DCD at different concentrations); Table S5 (Number of alive and dead cells of *N. europaea* in the absence and presence of DMP and DCD at different concentrations determined with a bacterial viability stain), Supplementary Figure S1 (O_2 consumption by *N. europaea* as a function of time in the absence of NI); Figure S2 (O_2 consumption by *N. europaea* as a function of time after the addition of DMP at different concentrations); Figure S3 (O_2 consumption by *N. europaea* as a function of time after the addition of DCD at different concentrations).

Author Contributions

S. C. Y performed the experiments, processed the experimental data and performed the analysis. R. W., U. R. and U. W. designed, planned and supervised the work. All authors aided in interpreting the results. S. C. Y. and U. W. wrote the manuscript and designed the figures with input of all authors.

Acknowledgement

We thank Sneha Gupta, Michelle Watt, Claudia Knief and Nicolas Brüggemann for helpful discussions and Guy Jamesson for providing the Clark Type Electrode. Support by the Bio21 Institute's Magnetic Resonance, and the Mass Spectrometry and Proteomics Facility (MSPF), Melbourne University and the School of BioSciences Microscopy Unit, are gratefully acknowledged.

Funding Sources

This work was supported by the Australian Research Council through the ARC Research Hub for Smart Fertilizers (IH200100023) and the Discovery Project ("Connecting soil nitrogen and plant uptake for greener agriculture", DP200101162) Schemes.

References

1. Food and Agriculture Organization of the United Nations (FAO). *World Fertilizer Trends and Outlook to 2020*. Rome, 2019. <http://www.fao.org/3/ca6746en/ca6746en.pdf> (accessed 2022-09-09).
2. Raun, W. R.; Schepers, J. S. Nitrogen Management for Improved Use Efficiency. In: *Nitrogen in Agricultural Systems* (Schepers, J. S.; Raun, W. R., eds.). **2008**, pp 675-693. DOI 10.2134/agronmonogr49.c17
3. Cavigelli, M. A.; Del Grosso, S. J.; Liebig, M. A.; Snyder, C. S.; Fixen, P. E.; Venterea, R. T.; Leytem, A. B.; McLain, J. E.; Watts, D. B. US Agricultural Nitrous Oxide Emissions: Context, Status, and Trends. *Front. Ecol. Environ.* **2012**, *10*, 537-546. DOI: 10.1890/120054

4. Ladha, J. K.; Pathak, H.; J. Krupnik, T.; Six, J.; van Kessel, C. Efficiency of Fertilizer Nitrogen in Cereal Production: Retrospects and Prospects. In: *Advances in Agronomy* Vol. 87; Academic Press, **2005**, pp 85-156. DOI 10.1016/S0065-2113(05)87003-8
5. Robertson, G. P.; Bruulsema, T. W.; Gehl, R. J.; Kanter, D.; Mauzerall, D. L.; Rotz, C. A.; Williams, C. O. Nitrogen–Climate Interactions in US Agriculture. *Biogeochemistry* **2013**, *114*, 41-70. DOI: 10.2307/24715091
6. Norton, J.; Ouyang, Y. Controls and Adaptive Management of Nitrification in Agricultural Soils. *Front. Microbiol.* **2019**, *10*, 1931. DOI: 10.3389/fmicb.2019.01931
7. Jetten, M. S. M. The Microbial Nitrogen Cycle. *Environ. Microbiol.* **2008**, *10*, 2903-2909. DOI: 10.1111/j.1462-2920.2008.01786.x
8. Coskun, D.; Britto, D. T.; Shi, W.; Kronzucker, H. J. Nitrogen Transformations in Modern Agriculture and the Role of Biological Nitrification Inhibition. *Nature Plants* **2017**, *3*, 17074. DOI: 10.1038/nplants.2017.74
9. Ruser, R.; Schulz, R. The Effect of Nitrification Inhibitors on the Nitrous Oxide (N₂O) Release from Agricultural Soils—a Review. *J. Plant Nutr. Soil Sci.* **2015**, *178*, 171-188. DOI: 10.1002/jpln.201400251

10. Lawton, T. J.; Ham, J.; Sun, T.; Rosenzweig, A. C. Structural Conservation of the B Subunit in the Ammonia Monooxygenase/Particulate Methane Monooxygenase Superfamily. *Proteins* **2014**, *82*, 2263-2267. DOI: 10.1002/prot.24535
11. McTavish, H.; Fuchs, J. A.; Hooper, A. B. Sequence of the Gene Coding for Ammonia Monooxygenase in *Nitrosomonas europaea*. *J. Bacteriol.* **1993**, *175*, 2436. DOI: 10.1128/jb.175.8.2436-2444.1993
12. Musiani, F.; Broll, V.; Evangelisti, E.; Ciurli, S. The Model Structure of the Copper-Dependent Ammonia Monooxygenase. *J. Biol. Inorg. Chem.* **2020**, *25*, 995-1007. DOI: 10.1007/s00775-020-01820-0
13. McCarty, G. W. Modes of Action of Nitrification Inhibitors. *Biol. Fertil. Soils* **1999**, *29*, 1-9. DOI: 10.1007/s003740050518
14. Hyman, M. R.; Sansome-Smith, A. W.; Shears, J. H.; Wood, P. M. A Kinetic Study of Benzene Oxidation to Phenol By Whole Cells of *Nitrosomonas europaea* and Evidence for the Further Oxidation of Phenol to Hydroquinone. *Arch. Microbiol.* **1985**, *143*, 302-306. DOI: 10.1007/BF00411254
15. Vajrala, N.; Martens-Habbena, W.; Sayavedra-Soto, L. A.; Schauer, A.; Bottomley, P. J.; Stahl, D. A.; Arp, D. J. Hydroxylamine as an Intermediate in Ammonia Oxidation by Globally Abundant Marine Archaea. *Proc. Natl. Acad. Sci.* **2013**, *110*, 1006-1011. DOI: 10.1073/pnas.1214272110

16. Sun, D.; Tang, X.; Zhao, M.; Zhang, Z.; Hou, L.; Liu, M.; Wang, B.; Klümper, U.; Han, P. Distribution and Diversity of Comammox Nitrospira in Coastal Wetlands of China. *Front. Microbiol.* **2020**, *11*, 589268. DOI: 10.3389/fmicb.2020.589268
17. Caranto, J. D.; Lancaster, K. M. Nitric Oxide is an Obligate Bacterial Nitrification Intermediate Produced by Hydroxylamine Oxidoreductase. *Proc. Natl. Acad. Sci.* **2017**, *114*, 8217-8222. DOI: 10.1073/pnas.170450411
18. Caranto, J. D.; Vilbert, A. C.; Lancaster, K. M. *Nitrosomonas europaea* Cytochrome P460 is a Direct Link Between Nitrification and Nitrous Oxide Emission. *Proc. Natl. Acad. Sci.* **2016**, *113*, 14704–14709. DOI: 10.1073/pnas.1611051113
19. Venterea, R. T.; Rolston, D. E. Mechanisms and Kinetics of Nitric and Nitrous Oxide Production During Nitrification in Agricultural Soil. *Glob. Chang. Biol.* **2000**, *6*, 303-316. DOI: 10.1046/j.1365-2486.2000.00309.x
20. Wrage-Mönnig, N.; Horn, M. A.; Well, R.; Müller, C.; Velthof, G.; Oenema, O. The Role of Nitrifier Denitrification in the Production of Nitrous Oxide Revisited. *Soil Biol. Biochem.* **2018**, *123*, A3–A16. DOI: 10.1016/j.soilbio.2018.03.020
21. Venterea, R. T.; Clough, T. J.; Coulter, J. A.; Souza, E. F. C.; Breuillin-Sessoms, F.; Spokas, K. A.; Sadowsky, M. J.; Gupta, S. K.; Bronson, K. F. Temperature Alters Dicyandiamide (DCD) Efficacy for Multiple Reactive Nitrogen Species in Urea-Amended Soils: Experiments and Modeling. *Soil Biol. Biochem.* **2021**, *160*, 108341. DOI: [10.1016/j.soilbio.2021.108341](https://doi.org/10.1016/j.soilbio.2021.108341)

22. Ensign, S. A.; Hyman, M. R.; Arp, D. J. *In vitro* Activation of Ammonia Monooxygenase from *Nitrosomonas europaea* by Copper. *J. Bacteriol.* **1993**, *175*, 1971-1980. DOI: 10.1128/jb.175.7.1971-1980.1993
23. Lieberman, R. L.; Rosenzweig, A. C. Crystal Structure of a Membrane-Bound Metalloenzyme that Catalyses the Biological Oxidation of Methane. *Nature* **2005**, *434*, 177-182. DOI: 10.1038/nature03311
24. Cao, L.; Caldararu, O.; Rosenzweig, A. C.; Ryde, U. Quantum Refinement Does Not Support Dinuclear Copper Sites in Crystal Structures of Particulate Methane Monooxygenase. *Angew. Chem. Int. Ed.* **2018**, *57*, 162-166. DOI: 10.1002/anie.201708977
25. Hyman, M. R.; Wood, P. M. Suicidal Inactivation and Labelling of Ammonia Monooxygenase by Acetylene. *Biochem. J.* **1985**, *227*, 719-725. DOI: 10.1042/bj2270719
26. Juliette, L. Y.; Hyman, M. R.; Arp, D. J. Inhibition of Ammonia Oxidation in *Nitrosomonas europaea* by Sulfur Compounds: Thioethers Are Oxidized to Sulfoxides by Ammonia Monooxygenase. *Appl. Environ. Microbiol.* **1993**, *59*, 3718-3727. DOI: 10.1128/aem.59.11.3718-3727.1993
27. Zhu, G.; Ju, X.; Zhang, J.; Müller, C.; Rees, R. M.; Thorman, R. E.; Sylvester-Bradley, R. Effects of the Nitrification Inhibitor DMPP (3,4-Dimethylpyrazole Phosphate) on Gross N

Transformation Rates and N₂O Emissions. *Biol. Fertil. Soils* **2019**, *55*, 603-615. DOI: 10.1007/s00374-019-01375-6

28. Li, H.; Liang, X.; Chen, Y.; Lian, Y.; Tian, G.; Ni, W. Effect of Nitrification Inhibitor DMPP on Nitrogen Leaching, Nitrifying Organisms, and Enzyme Activities in a Rice-Oilseed Rape Cropping System. *J. Environ. Sci.* **2008**, *20*, 149-155. DOI: 10.1016/S1001-0742(08)60023-6

29. Guardia, G.; Marsden, K. A.; Vallejo, A.; Jones, D. L.; Chadwick, D. R. Determining the Influence of Environmental and Edaphic Factors on the Fate of the Nitrification Inhibitors DCD and DMPP in Soil. *Sci. Total Environ.* **2018**, *624*, 1202-1212. DOI: 10.1016/j.scitotenv.2017.12.250

30. Barrena, I.; Menéndez, S.; Correa-Galeote, D.; Vega-Mas, I.; Bedmar, E. J.; González-Murua, C.; Estavillo, J. M. Soil Water Content Modulates the Effect of the Nitrification Inhibitor 3,4-Dimethylpyrazole Phosphate (DMPP) on Nitrifying and Denitrifying Bacteria. *Geoderma* **2017**, *303*, 1-8. DOI: 10.1016/j.geoderma.2017.04.022

31. Koci, J.; Nelson, P. N. Tropical Dairy Pasture Yield and Nitrogen Cycling: Effect of Urea Application Rate and a Nitrification Inhibitor, DMPP. *Crop Pasture Sci.* **2016**, *67*, 766-779. DOI: 10.1071/CP15400

32. Menéndez, S.; Merino, P.; Pinto, M.; González-Murua, C.; Estavillo, J. M. 3,4-Dimethylpyrazol Phosphate Effect on Nitrous Oxide, Nitric Oxide, Ammonia, and Carbon Dioxide Emissions from Grasslands. *J. Environ. Qual.* **2006**, *35*, 973-981. DOI: 10.2134/jeq2005.0320

33. Dougherty, W. J.; Collins, D.; Van Zwieten, L.; Rowlings, D. W. Nitrification (DMPP) and Urease (NBPT) Inhibitors Had No Effect on Pasture Yield, Nitrous Oxide Emissions, or Nitrate Leaching under Irrigation in a Hot-Dry Climate. *Soil Res.* **2016**, *54*, 675-683. DOI: 10.1071/SR15330
34. Weiske, A.; Benckiser, G.; Ottow, J. C. G. Effect of the New Nitrification Inhibitor DMPP in Comparison to DCD on Nitrous Oxide (N₂O) Emissions and Methane (CH₄) Oxidation During 3 Years of Repeated Applications in Field Experiments. *Nutr. Cycling Agroecosyst.* **2001**, *60*, 57-64. DOI: 10.1023/A:1012669500547
35. Lin, X.; Hasi, W.-L.-J.; Lou, X.-T.; Han, S.-q.-g.-w.; Lin, D.-Y.; Lu, Z.-W. Direct and Quantitative Detection of Dicyandiamide (DCD) in Milk Using Surface-Enhanced Raman Spectroscopy. *Anal. Meth.* **2015**, *7*, 3869-3875. DOI: 10.1039/C5AY00313J
36. Chen, Q.; Qi, L.; Bi, Q.; Dai, P.; Sun, D.; Sun, C.; Liu, W.; Lu, L.; Ni, W.; Lin, X. Comparative Effects of 3,4-Dimethylpyrazole Phosphate (DMPP) and Dicyandiamide (DCD) on Ammonia-Oxidizing Bacteria and Archaea in a Vegetable Soil. *Appl. Microbiol. Biotechnol.* **2015**, *99*, 477-487. DOI: 10.1007/s00253-014-6026-7
37. Vannelli, T.; Hooper, A. B. Oxidation of Nitrapyrin to 6-Chloropicolinic Acid by the Ammonia-Oxidizing Bacterium *Nitrosomonas europaea*. *Appl. Environ. Microbiol.* **1992**, *58*, 2321-2325. DOI: 10.1128/aem.58.7.2321-2325.1992

38. Campbell, N. E. R.; Aleem, M. I. H. The Effect of 2-Chloro, 6-(Trichloromethyl) Pyridine on the Chemoautotrophic Metabolism of Nitrifying Bacteria. *Antonie Van Leeuwenhoek* **1965**, *31*, 124-136. DOI: 10.1007/BF02045882
39. Woodward, E. E.; Edwards, T. M.; Givens, C. E.; Kolpin, D. W.; Hladik, M. L. Widespread Use of the Nitrification Inhibitor Nitrapyrin: Assessing Benefits and Costs to Agriculture, Ecosystems, and Environmental Health. *Environ. Sci. Technol.* **2021**, *55*, 1345-1353. DOI: 10.1021/acs.est.0c05732
40. Corrochano-Monsalve, M.; González-Murua, C.; Bozal-Leorri, A.; Lezama, L.; Artetxe, B. Mechanism of Action of Nitrification Inhibitors Based on Dimethylpyrazole: A Matter of Chelation. *Sci. Total Environ.* **2021**, *752*, 141885. DOI: 10.1016/j.scitotenv.2020.141885
41. Amberger, A. Research on Dicyandiamide as a Nitrification Inhibitor and Future Outlook. *Commun. Soil Sci. Plant Anal.* **1989**, *20*, 1933-1955. DOI: 10.1080/00103628909368195
42. Hooper, A. B.; Terry, K. R. Specific Inhibitors of Ammonia Oxidation in *Nitrosomonas*. *J. Bacteriol.* **1973**, *115*, 480-485. DOI: 10.1128/jb.115.2.480-485.1973
43. Casali, L.; Feiler, T.; Heilmann, M.; Braga, D.; Emmerling, F.; Grepioni, F. Too Much Water? Not Enough? In Situ Monitoring of the Mechanochemical Reaction of Copper Salts with Dicyandiamide. *CrystEngComm* **2022**, *24*, 1292-1298. DOI: 10.1039/D1CE01670A

44. Yildirim, S. C.; Walker, R. M.; Roessner, U.; Wille, U. A Rapid and Inexpensive Assay for Testing the Efficiency of Potential New Synthetic Nitrification Inhibitors. *Submitted*.
45. Wise, R. R.; Naylor, A. W. Calibration and Use of a Clark-Type Oxygen Electrode from 5 to 45 degrees C. *Anal. Biochem.* **1985**, *146*, 260-264. DOI: 10.1016/0003-2697(85)90424-5.
46. GraphPad Prism version 9.5.0 for Windows, GraphPad Software, San Diego, California USA, www.graphpad.com.
47. Subbarao, G. V.; Ishikawa, T.; Ito, O.; Nakahara, K.; Wang, H. Y.; Berry, W. L. A Bioluminescence Assay to Detect Nitrification Inhibitors Released From Plant Roots: A Case Study with *Brachiaria humidicola*. *Plant Soil* **2006**, *288*, 101-112. DOI: 10.1007/s11104-006-9094-3
48. O'Sullivan, C. A.; Duncan, E. G.; Whisson, K.; Treble, K.; Ward, P. R.; Roper, M. M. A Colourimetric Microplate Assay for Simple, High Throughput Assessment of Synthetic and Biological Nitrification Inhibitors. *Plant Soil* **2017**, *413*, 275-287. DOI: 10.1007/s11104-016-3100-1
49. Daugherty, N. A.; Swisher, J. H. Metal Complexes of Pyrazole. *Inorg. Chem.* **1968**, *7*, 1651-1653. DOI: 10.1021/ic50066a039
50. Delaune, K. P.; Alsayouri, K. *Physiology, Noncompetitive Inhibitor*. In: *StatPearls Publishing [internet]*. StatPearls Publishing 2022. (accessed 2022-10-04).

51. Fisher, O. S.; Kenney, G. E.; Ross, M. O.; Ro, S. Y.; Lemma, B. E.; Batelu, S.; Thomas, P. M.; Sosnowski, V. C.; DeHart, C. J.; Kelleher, N. L.; Stemmler, T. L.; Hoffman, B. M.; Rosenzweig, A. C. Characterization of a Long Overlooked Copper Protein from Methane- and Ammonia-Oxidizing Bacteria. *Nat. Commun.* **2018**, *9*, 4276. DOI: 10.1038/s41467-018-06681-5
52. Wright, C. L.; Schatteman, A.; Crombie, A. T.; Murrell, J. C.; Lehtovirta-Morley, L. E.; Stams, A. J. M. Inhibition of Ammonia Monooxygenase from Ammonia-Oxidizing Archaea by Linear and Aromatic Alkynes. *Appl. Environ. Microbiol.* **2020**, *86*, e02388-02319. DOI: doi:10.1128/AEM.02388-19
53. Arp, D. J.; Sayavedra-Soto, L. A.; Hommes, N. G. Molecular Biology and Biochemistry of Ammonia Oxidation by *Nitrosomonas europaea*. *Arch. Microbiol.* **2002**, *178*, 250-255. DOI: 10.1007/s00203-002-0452-0
54. Keener, W. K.; Russel, S. A.; Arp, D. J. Kinetic Characterization of the Inactivation of Ammonia Monooxygenase in *Nitrosomonas europaea* by Alkyne, Aniline and Cyclopropane Derivatives. *Biochim. Biophys. Acta Proteins Proteom.* **1998**, *1388*, 373-385. DOI: 10.1016/S0167-4838(98)00188-5
55. Lontoh, S.; DiSpirito, A. A.; Krema, C. L.; Whittaker, M. R.; Hooper, A. B.; Semrau, J. D. Differential Inhibition *In Vivo* of Ammonia Monooxygenase, Soluble Methane Monooxygenase and Membrane-Associated Methane Monooxygenase by Phenylacetylene. *Environ. Microbiol.* **2000**, *2*, 485-494. DOI: 10.1046/j.1462-2920.2000.00130.x

56. Arnaout, C. L.; Gunsch, C. K. Impacts of Silver Nanoparticle Coating on the Nitrification Potential of *Nitrosomonas europaea*. *Environ. Sci. Technol.* **2012**, *46*, 5387-5395. DOI:
57. Mahmood, T.; Rehmat, A.; Asma, L.; Muhammad, S. (2017) 4-Amino-1,2,4-Triazole Can be More Effective Than Commercial Nitrification Inhibitors at High Soil Temperatures. *Soil. Res.* **2017**, *55*, 715-722. DOI: 10.1071/SR16340
58. Kelliher, F.M.; Clough, T. J.; Clark, H.; Rys, G.; Sedcole, J. R. The Temperature Dependence of Dicyandiamide (DCD) Degradation in Soils: A Data Synthesis. *Soil Biol. Biochem.* **2008**, *40*, 1878–1882. DOI: 10.1016/j.soilbio.2008.03.013

Table of Contents Graphic

